Hindawi
Advances in Materials Science and Engineering
Volume 2019, Article ID 9465730, 8 pages
https://doi.org/10.1155/2019/9465730

Research Article

Study of Structural Properties of BiOI on ZnO Thin Films and ZnO Nanorods

C. D. Gutiérrez-Lazos,[1] **A. Fundora-Cruz**,[2] **F. Solís-Pomar**,[1] **and E. Pérez-Tijerina**[1]

[1]*Centro de Investigación en Ciencias Físico Matemáticas, Facultad de Ciencias Físico Matemáticas, Universidad Autónoma de Nuevo León, Av. Universidad s/n. Ciudad Universitaria, 66451 San Nicolás de los Garza, Nuevo León, Mexico*
[2]*Instituto de Ciencia y Tecnología de Materiales (IMRE), Universidad de La Habana, Zapata y G. Vedado, 10400 La Habana, Cuba*

Correspondence should be addressed to C. D. Gutiérrez-Lazos; claudio.gutierrezl@uanl.edu.mx

Received 29 November 2018; Revised 18 February 2019; Accepted 25 February 2019; Published 3 April 2019

Academic Editor: Davide Palumbo

We report the study of ZnO nanorods (ZnO-NR) decorated with BiOI nanoplatelets by the simple precipitation of BiOI in aqueous solution containing ZnO-NR powders. Likewise, as a reference for the decoration of ZnO-NR, BiOI thin films were prepared by the SILAR technique on RF magnetron-sputtered ZnO thin films. The scanning electron microscopy analysis showed that BiOI grew on the ZnO-NR surfaces in nanoplatelet shape with an order of magnitude smaller in size, with respect to the platelets observed in BiOI thin films. Analysis by X-ray diffraction exhibited the hexagonal $P6_3mc$ phase of ZnO and the tetragonal P_4nmm crystal phase of BiOI. On the other hand, BiOI thin films are nonuniform and strongly adherent and, besides they exhibited the P_4nmm tetragonal crystal structure of BiOI, they have highly preferential orientation along (001) direction (9.66°). Optical characterization of ZnO-NR/BiOI by absorbance showed a widened peak slightly shifted to infrared compared with the ZnO-NR absorbance peak, suggesting the increase of the absorption wavelength ranges from the ultraviolet to visible for ZnO-NR. Similarly, the results of the optical characterization by absorbance, for BiOI thin films, indicated the bandgap energy of the samples was between 1.78 eV and 1.88 eV, values previously reported for BiOI.

1. Introduction

The importance of ZnO material is well known due to its excellent physicochemical properties, which we can mention, and its thermal and mechanical stability that allows ZnO to crystallize in different morphologies, microstructured and nanostructured; its wide bandgap energy (3.37 eV), its high optical absorption (300 cm^{-1}), its large exciton bond power of 60 meV, and its high speed to generate electron-hole pairs under optical excitation make the ZnO have excellent photocatalytic properties as an oxidant under UV irradiation, when it is synthesized in nanostructures [1–3]. However, a limiting factor in its photocatalytic performance is the narrow range of energies of the electromagnetic spectrum required to activate the photocatalysis [4, 5]. In this way, in order to take advantage of a greater range of the solar spectrum, it is necessary to combine ZnO with other materials with photocatalytic properties that require a lower energy to work. An excellent candidate to extend the energy range of photocatalytic activation is BiOI, which has a narrow bandgap energy from 1.6 to 1.9 eV [6–8] and has a tetragonal crystal structure, belonging to the P_4nmm group, which offers important advantages such as the formation of internal electric fields that separate the photogenerated electron-hole pairs and prevent their recombination. This field is formed by the way BiOI is structured, according to its Bravais cell exhibited in Figure 1, in which layers of $(Bi_2O_2)^{2+}$ and iodide ion bilayers (I^-) are intercalated [9, 10].

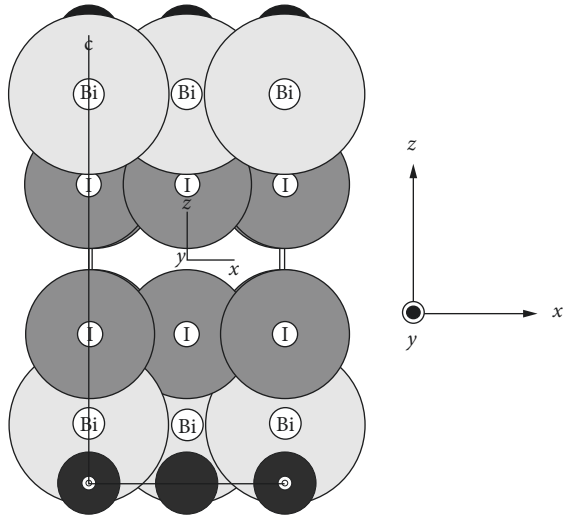

Figure 1: Schematic representation of the Bravais cell for BiOI.

The most effective photocatalytic applications reported for BiOI are based on n-p inorganic nanocomposites such as TiO_2/BiOI [11], ZnO/BiOI [12], and Bi_2S_3/BiOI [13], among others [14–16], both powder and as thin film. The preparation of BiOI thin films has been reported on porous surfaces, mainly TiO_2 by spray pyrolysis or SILAR techniques [17, 18], on ZnO nanorods films as a decoration [19], by using the solvothermal technique at temperatures above 100°C always employing ethylene glycol as the solvent.

In this research, we report for the first time a systematic study of the structural properties of BiOI synthesized entirely in aqueous medium at room temperature. Our study begins with BiOI thin films grown by the SILAR method on RF magnetron-sputtered ZnO thin films and continues with powder samples, obtained by the precipitation of BiOI in aqueous medium. Likewise, we report a relatively simple process to decorate ZnO nanorods by precipitin BiOI from a simple chemical reaction between two aqueous solutions, the first one of $Bi(NO_3)_2$ and the second one a solution containing powders of ZnO nanorods dispersed in aqueous solution of KI.

2. Experimental

2.1. Materials. Zinc nitrate hexahydrate ($Zn(NO_3)_3{\cdot}6H_2O$, Sigma-Aldrich, reagent grade, 98%), hexamethylenetetramine (hexamine, $(CH_2)_6{\cdot}N_4$, Sigma-Aldrich, ACS reagent, ≥99.0%), bismuth (III) nitrate pentahydrate (Sigma-Aldrich, ACS reagent, ≥98.0%), and potassium iodide (Sigma-Aldrich, anhydrous, 99%).

2.2. Synthesis of BiOI. In order to characterize the structural and optical properties of BiOI, we prepared a group of samples as thin films by employing the SILAR technique [20]. The BiOI thin films were grown on ZnO, deposited by the sputtering technique on commercial glass substrates by 40, 90, and 120 immersion cycles. The ZnO thin film was initially immersed in 20 mL of an aqueous solution of 0.2 M $Bi(NO_3)_2$ for 2 min; afterwards, the sample was removed, washed with deionized water, and dried with N_2. Then, the sample was immersed in 20 mL of an aqueous solution of 0.2 M KI, also for 2 min. Immediately after, the sample was removed, washed, and dried with deionized water and N_2, respectively, in order to restart a new cycle of immersion.

A second group of samples was prepared as powders; these samples were synthesized by mixing, under strong magnetic agitation, 0.2 M $Bi(NO_3)_2$ (2 mL) and a solution of 0.2 M KI (2 mL) dissolved in 0 mL, 40 mL, 80 mL, and 160 mL (powder samples 1, 2, 3, and 4, respectively) of deionized water. The precipitated solid was separated from the solution and dried in an oven at 100°C.

2.3. Synthesis of ZnO Nanorods. ZnO-NR powders were synthesized by the hydrothermal method based on an equimolar reaction of 0.01 M $Zn(NO_3)_3{\cdot}6H_2O$ and hexamethylenetetramine in aqueous medium, at 90°C for 4 h. The solid phase was separated by centrifugation and dried in an oven (80°C).

2.4. Decoration of ZnO-NR. Decorated ZnO-NR were prepared by the precipitation of BiOI on ZnO-NR powders at room temperature. A sample of 29 mg ZnO-NR was initially dispersed in 2 mL of an aqueous solution of 0.2 M KI under ultrasonic agitation. Deionized water (38 mL) was added, and immediately after, 2 mL of an aqueous solution of 0.02 M $Bi(NO_3)_2$ was supplied. The mixture turned to a yellow turbid and was maintained at room temperature and under magnetic agitation for 5 min. The solid phase was separated and dried in an oven (100°C).

2.5. Characterization. Morphology of BiOI thin films and ZnO-NR/BiOI nanostructures were analyzed by scanning electron microscopy (SEM) employing a Jeol JSM 5200 microscope. The structural analysis was realized by X-ray diffraction by using a PANalytical X'Pert³ Powder system at 45 kV and 40 mA, and the optical characterization was realized in an Evolution 600 UV–visible Thermo Fisher Scientific spectrometer.

3. Results and Discussion

3.1. SEM Analysis

3.1.1. BiOI Samples. Based on SEM analysis, BiOI thin films exhibit a nonuniform surface predominantly formed by microplatelets grown in perpendicular direction with respect to the substrate surface as we can see in Figures 2(a) and 2(b).

The different crystalline shapes observed in the micrographs of Figures 2(a) and 2(b) suggest different growth stages of a BiOI thin film on a ZnO deposition. According to this observation, in its first stage, BiOI precipitates in hemispherical grains formed by platelets as exhibited in the inset of Figure 2(a) with a mean size of 3 μm. A second stage can be explained on the main micrograph of Figure 2(a), where we can observe areas with a greater concentration of these hemispherical grains, which continue to grow overlapping each other until the surface is built, as shown in

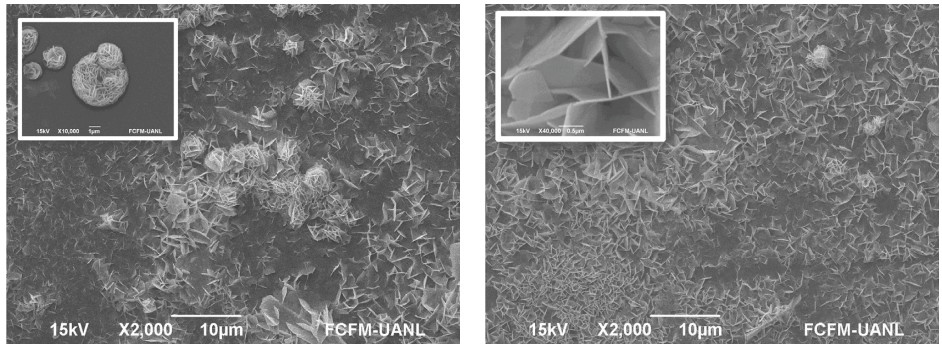

(a) (b)

Figure 2: SEM micrographs corresponding to a BiOI thin film grown on a ZnO thin film. It is possible to observe different stages of growth: (a) the growth of rounded grains and their overlapping and (b) microplatelets grown in perpendicular direction to the substrate surface.

Figure 2(b). The inset of Figure 2(b) exhibits an amplification of the final surface of the sample.

The microstructure exhibited in the inset of Figure 2(a) has been reported by several authors who precipitated BiOI by solvothermal technique in aqueous solution of glycol and ethylene glycol [8, 21, 22]. Similarly, Hahn et al. reported a nonuniform BiOI thin film deposited by spray pyrolysis by using ethylene glycol solutions of $Bi(NO_3)_2$ and NH_4I as precursors [17]. The thin films showed a dependence with the grown temperature both in size and shape. According to other authors, in all depositions realized at different temperatures of substrates, growth of nanoplatelets was observed vertically. Although the highly oriented growth is not verified by X-ray diffraction analysis, TEM micrography exhibits the nanoplatelets oriented in normal direction to the substrate [17]. A similar surface was obtained by Bhachu et al. [23]. In the present work, we have obtained a BiOI thin film formed by highly oriented microplatelets by employing the SILAR technique at room temperature through the reaction of $Bi(NO_3)_2$ and KI on the substrate surface.

3.1.2. Decoration of ZnO-NR. The result of decorating ZnO-NR with BiOI nanoplates is shown in Figures 3(a) and 3(b). According to these micrographs, we could assume that ZnO-NR surfaces are serving as seeds for the growth of BiOI nanoplatelets. We can verify that practically all nanorods prepared by the hydrothermal method exhibit a high concentration of BiOI nanoplatelets on their surfaces, and the nanoplatelets, such as in BiOI thin films, are oriented in perpendicular direction with respect to nanorod surfaces.

In the inset of Figure 3(b), we calculated the extension of these nanostructures and found that these were reduced by an order of magnitude with respect to growth of BiOI plates on ZnO thin films since the surface in which actually BiOI grows is micrometric. Thus, we have obtained micrometric ZnO nanorods decorated by BiOI nanoplates vertically oriented with respect to ZnO nanorod surface.

Kuang et al. [19] reported the growth of ZnO-NR on fluorine-doped tin oxide which was decorated by BiOI nanoplatelets through a solvothermal method at 126°C, for 6 h. Other reports have published the preparation of ZnO/BiOI nanocomposites by one-pot synthesis of ZnO and BiOI precursors heated in an autoclave, also around 125°C [24] or by microwave irradiation [25]; however, reports about nanocomposites formed by ZnO nanorods decorated with BiOI micro/nanoplatelets, or with a shell of BiOI, are rare. Hence, we are reporting a simple process of preparation at room temperature of decorated ZnO nanorods by BiOI nanoplatelets through the simple dispersion of ZnO-NR in aqueous solution of 0.2 M KI and adding an aqueous solution of 0.02 M $Bi(NO_3)_2$.

3.2. X-ray Diffraction. The X-ray diffraction patterns exhibited in Figure 4 correspond to BiOI samples grown on ZnO thin films by 40, 90, and 120 SILAR immersion cycles (labeled as 40, 90, and 120 cycles). One of these samples was annealed at 100°C, as is indicated in Figure 5. In addition, we also have the X-ray diffraction patterns for powder samples synthesized according to the method described in Section 2.2. All diffraction patterns were obtained for 2Θ values from 5 to 60°. In the diffractogram corresponding to 40 cycles sample, it is possible to observe a highly intense peak around 9.66° and a series of lower intensity peaks in 19.39, 29.74, 39.49, 45.78, 51.63, and 55.42°. All peaks correspond to reflections of the crystalline planes (001), (002), (004), (200), (211), and (105)/(212) of the tetragonal phase (group P_4nmm) of BiOI [26]. The same crystalline phase was also observed for all samples, both thin film and powder. The intensity of the observed peaks is reduced for the 90 and 120 cycle samples, possibly due to the dissolution of thin film surface with the successive SILAR cycles, which causes the reduction of their thickness. The thermal treatment of the sample prepared by 40 SILAR cycles has reduced the intensity of the (001) peak and has been increasing slightly the intensity of the remaining peaks. According to the texture coefficient, $f(hkl)$ [27],

$$f(hkl) = \frac{I(hkl)/I_0(hkl)}{\sum_{i=1}^{N} I_i(hkl)/I_0(hkl)}, \quad (1)$$

where $I_0(hkl)$ and $I(hkl)$ are the standard X-ray intensity of BiOI and the measured X-ray intensity corresponding to the hkl crystalline plane; the $f(001)$ factor is 2.47 for the sample

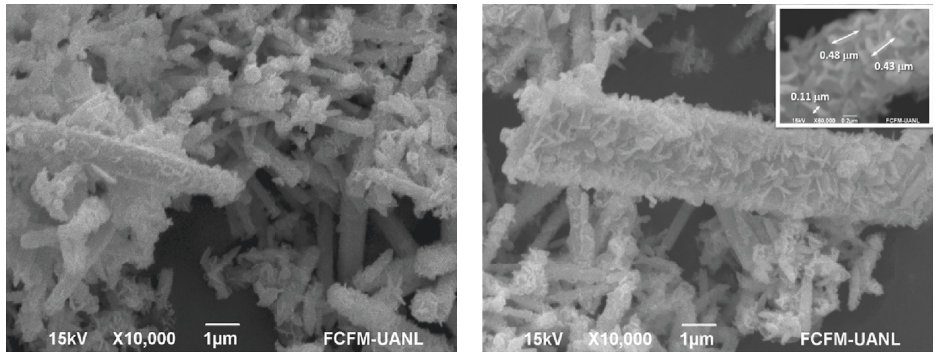

(a) (b)

Figure 3: SEM micrograph obtained from different positions of a powder sample of decorated ZnO nanorods. The inset in Figure 2(b) shows the size measurements of some nanoplatelets.

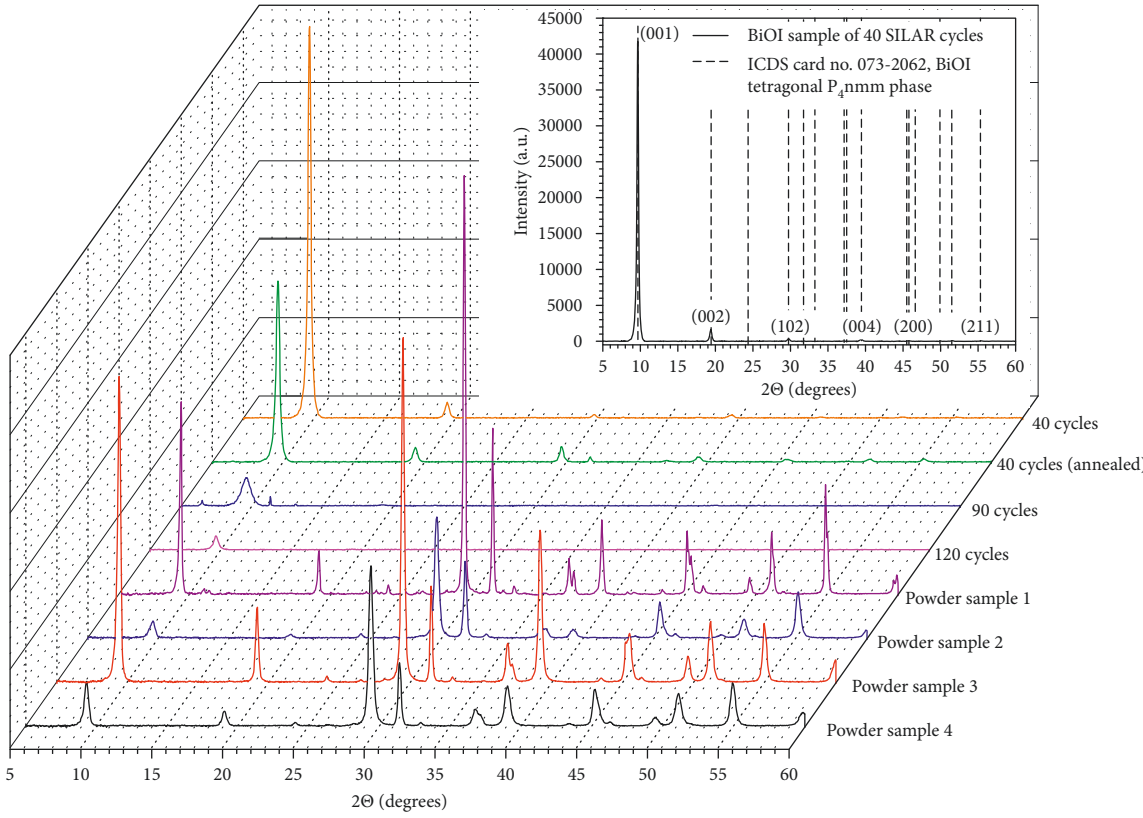

Figure 4: X-ray diffraction patterns corresponding to BiOI samples grown on ZnO thin films and BiOI powder samples.

of 40 SILAR cycles and $f(hkl) < 1$, for the other crystalline planes. The $f(001)$ factor is reduced to 0.95 with annealing; however, the preferential orientation of thin films crystal structure is highly directed along the plane (001). However, for all powder samples, the preferential orientation like that exhibited by thin film samples was not observed.

On the other hand, the (001) reflection, exhibited by all samples, rarely has been reported by other authors, and the high intensity showed in thin film samples has not been reported [21, 28]. Hence, the highly oriented BiOI microplatelets observed in the micrographs of Figure 2 is a consequence of the highly oriented crystal structure along (001) direction. Therefore, BiOI grows preferably perpendicular to the direction of the ZnO thin film surface, along (001) direction.

The X-ray diffraction pattern exhibited in Figure 5 corresponds to a powder sample of decorated ZnO-NR. We can easily distinguish two crystalline phases through two-line shapes, the first one, formed by broadened diffraction peaks of minor intensity, and the second one, formed by narrowed diffraction peaks of high intensity. The diffraction peaks of minor intensity correspond to BiOI

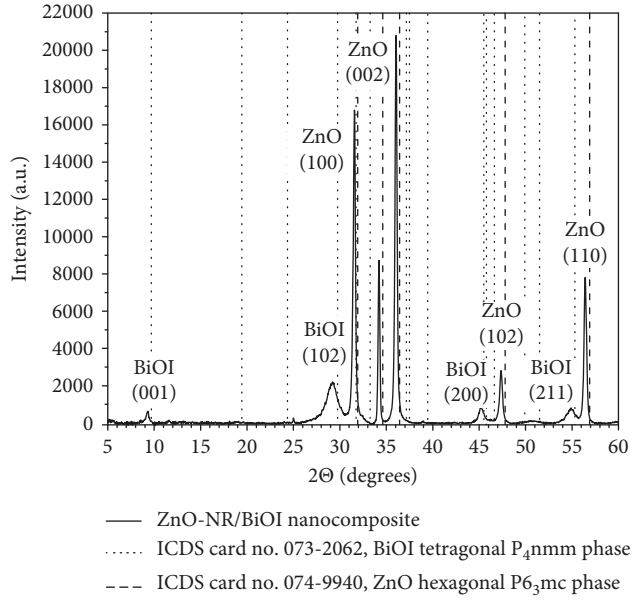

Figure 5: Diffraction pattern corresponding to decorated ZnO nanorods.

Table 1: Lattice parameters, interplanar spacing, and crystallite size measured for all samples.

Samples			d(Å)		FWHM-β		D (nm)	
	a (Å)	c (Å)	(001)	(102)	(001)	(102)	(001)	(102)
40 cycles	3.3888	9.1580	9.15804	3.00251	0.1791	0.2047	49	44
40 cycles of annealing	3.3977	9.2153	9.21532	3.01277	0.6140	0.4093	14	22
90 cycles	—	9.2100	9.21004		0.2047	—	42	—
120 cycles	—	9.1775	9.17754		0.3070	—	28	—
ICDS card 01-073-2062	**3.9840**	**9.1280**	**9.1280**	**3.00136**	—	—	—	—
Powder sample 1	3.4152	9.4326	9.4326	3.0399	0.1279	0.1535	68	58
Powder sample 2	3.4014	9.2101	9.21008	3.01496	0.2047	0.307	42	29
Powder sample 3	3.4096	9.3989	9.3989	3.03366	0.2047	0.2303	42	39
Powder sample 4	3.4090	9.5025	9.50251	3.04011	0.2814	0.3582	31	25
ZnO-NR/BiOI	3.4295	9.48934	9.48934	3.05372	0.1032	0.2047	84	44

nanoplatelets grown on ZnO-NR surface. Unlike the diffraction pattern of BiOI thin film showed in Figure 4, the diffraction peaks corresponding to BiOI nanoplatelets grown on the ZnO-NR surface are widened and shifted slightly to minor 2Θ values, possibly due to tensions in their crystal structure and the mismatch lattice parameters between the BiOI and ZnO-NR crystalline structures. Likewise, there is no preferential growth along (001) direction.

In order to compare the influence of the sample preparation method on the structural properties of BiOI, X-ray diffraction patterns were analyzed to obtain interplanar spacing, crystallite size, and lattice parameters. The interplanar spacing of tetragonal lattice was obtained by using the formula [29]:

$$\frac{1}{d_{hkl}^2} = \frac{(h^2 + k^2)}{a^2} + \frac{l^2}{c^2}, \tag{2}$$

where h, k, and l, are the Miller indexes and a and c are the lattice constants of the tetragonal lattice. The crystallite size was measured by the Debye–Scherrer formula [29]:

$$D = \frac{K\lambda}{\beta \cos \Theta}, \tag{3}$$

where K is the shape factor with value 0.9, λ is the wavelength of X-ray used (1.5418 Å), β is the full width at the maximum (FWHM) of the diffraction major line, and Θ is the Bragg angle. All values for lattice parameters, interplanar spacing, and crystallite size are listed in Table 1. In general, we can observe that BiOI has a crystal structure considerably stable, but interplanar spacing and the lattice parameters experienced only slight changes. These variations are observed mainly as a compression of the lattice cell through the axis a and b, with a slight elongation of the axis c. Important changes were not observed with other samples, including the ZnO-NR/BiOI, which means that BiOI is a compound relatively simple to obtain with a crystal structure highly stable. This characteristic allows its application as a photocatalyst both in aqueous and gas media, maintaining the same properties such as BiOI thin film, powder, and decorative on ZnO nanorod surface without employing

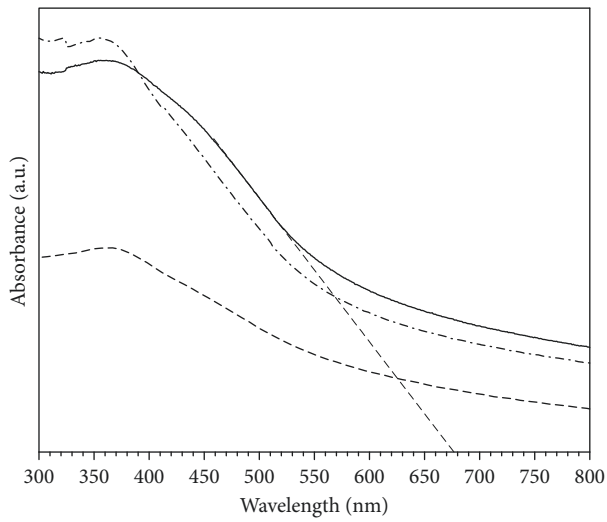

Figure 6: Absorbance spectrum of BiOI thin film grown by SILAR technique.

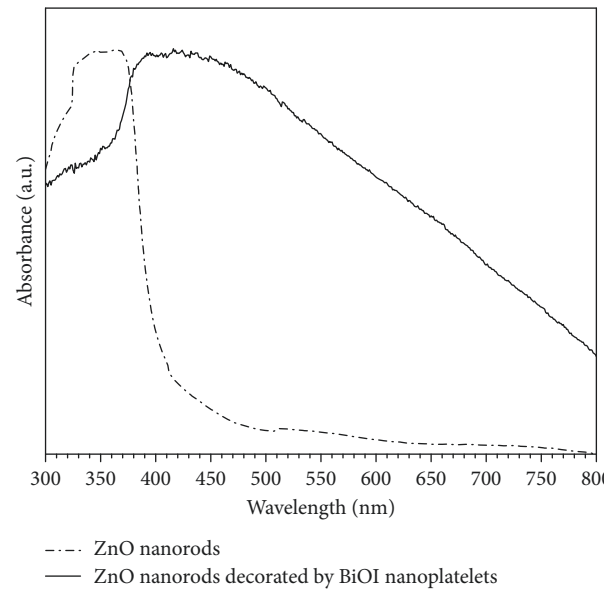

Figure 7: Absorbance spectra of ZnO-NR and ZnO-NR decorated by BiOI.

ethylene glycol or another organic compound. Furthermore, the crystallite size increased when BiOI is grown homogeneously, as powder, reaching its maximum value for the growth of BiOI on ZnO-NR surface.

3.3. Optical Properties. The optical absorption spectra for some representative BiOI thin films are shown in Figure 6. The samples were prepared by SILAR technique with 20, 30, and 120 immersion cycles on ZnO thin films. The bandgap of samples was calculated by the extrapolation of the straight line portion of the curves to zero absorbance value [30].

The bandgap value practically remained unchanged, within the range from 1.78 eV to 1.88 eV, which is close to values reported in other works [31]. This means that the wavelength interval of the optical absorption of ZnO-NR can be increased from the ultraviolet to visible band.

Figure 7 shows the absorbance spectrum of decorated and nondecorated ZnO-NR. We can observe the effect of BiOI growth on ZnO nanorods through its optical absorption since the main peak of the spectrum of ZnO is broadened and lightly shifted towards the infrared range of wavelength. This means that ZnO nanorods extended their spectrum of optical absorption from the ultraviolet to the visible.

4. Conclusions

We have reported the growth of BiOI nanostructures on ZnO nanorod surface through a simple precipitation of BiOI in aqueous solution containing ZnO nanorod powder at room temperature. The morphology analysis by scanning electron microscopy showed that nanorod surfaces worked as seed coatings for the growth of BiOI structures in nanoplatelet shape. Analysis by X-ray diffraction confirmed the observation by electron microscopy; the diffraction pattern of ZnO nanorods/BiOI powders exhibited the crystalline phases $P6_3mc$ (hexagonal) and P_4nmm (tetragonal) of ZnO and BiOI, respectively. Absorbance spectroscopy showed that ZnO nanorods extended their spectrum of optical absorption from the ultraviolet to the visible. BiOI thin films were nonuniform and formed mostly by microplatelets highly oriented in perpendicular direction with respect to the surface of ZnO film where they were grown. The preferential orientation of these structures was verified by X-ray diffraction technique, whose analysis indicated that BiOI films grew highly oriented in z direction, specifically along the (001) direction, and with a stable crystalline structure.

Data Availability

Authors declare no data were used to support this study.

Conflicts of Interest

The authors declare that there are no conflicts of interest regarding the publication of this paper.

Acknowledgments

The authors are grateful for the financial support of PRODEP through project DSA/103.5/16/10510.

Supplementary Materials

Graphical abstract: The left image is a SEM micrograph corresponding to BiOI thin films grown on a ZnO thin film, where it is possible to observe microplatelets grown in perpendicular direction to the substrate surface. The right

image corresponds to a SEM micrograph of a powder sample of decorated ZnO nanorods, where we can observe the growth of BiOI structures in nanoplatelet shape. (*Supplementary Materials*)

References

[1] W. Xitao, R. Lv, and W. Kang, "Synthesis of ZnO@ZnS–Bi_2S_3 core–shell nanorod grown on reduced graphene oxide sheets and its enhanced photocatalytic performance," *Journal of Materials Chemistry A*, vol. 2, no. 22, pp. 8304–8313, 2014.

[2] M. Mansournia, S. Rafizadeh, and S. M. Hosseinpour-Mashkani, "An ammonia vapor-based approach to ZnO nanostructures and their study as photocatalyst material," *Ceramics International*, vol. 42, no. 1, pp. 907–916, 2016.

[3] M. Mansournia, S. Rafizadeh, and S. M. Hosseinpour-Mashkani, "Hydrothermal synthesis, characterization and light harvesting applications of zinc oxide nanostructures," *Journal of Materials Science: Materials in Electronics*, vol. 26, no. 8, pp. 5839–5846, 2015.

[4] H. X. Sang, X. T. Wang, C. C. Fan, and F. Wang, "Enhanced photocatalytic H_2 production from glycerol solution over ZnO/ZnS core/shell nanorods prepared by a low temperature route," *International Journal of Hydrogen Energy*, vol. 37, no. 2, pp. 1348–1355, 2012.

[5] M. Mansournia, S. Rafizadeh, S. M. Hosseinpour-Mashkani, and M. H. Motaghedifard, "Novel room temperature synthesis of ZnO nanosheets, characterization and potentials in light harvesting applications and electrochemical devices," *Materials Science and Engineering: C*, vol. 65, pp. 303–312, 2016.

[6] J. Cao, B. Xu, B. Luo, H. Lin, and S. Chen, "Novel BiOI/BiOBr heterojunction photocatalysts with enhanced visible light photocatalytic properties," *Catalysis Communications*, vol. 13, no. 1, pp. 63–68, 2011.

[7] H. Liu, W. Cao, Y. Su, Y. Wang, and X. Wang, "Synthesis, characterization and photocatalytic performance of novel visible-light-induced Ag/BiOI," *Applied Catalysis B: Environmental*, vol. 111-112, pp. 271–279, 2012.

[8] Q. C. Liu, D. K. Ma, Y. Y. Hu, Y. W. Zeng, and S. M. Huang, "Various bismuth oxyiodide hierarchical architectures: alcohothermal-controlled synthesis, photocatalytic activities, and adsorption capabilities for phosphate in water," *ACS Applied Materials and Interfaces*, vol. 5, no. 22, pp. 11927–11934, 2013.

[9] R. He, S. Cao, P. Zhou, and J. Yu, "Recent advances in visible light Bi-based photocatalysts," *Chinese Journal of Catalysis*, vol. 35, no. 7, pp. 989–1007, 2014.

[10] J. Su, Y. Xiao, and M. Ren, "Direct hydrolysis synthesis of BiOI flowerlike hierarchical structures and it's photocatalytic activity under simulated sunlight irradiation," *Catalysis Communications*, vol. 45, pp. 30–33, 2014.

[11] B. Krishnakumar, R. Hariharan, V. Pandiyan, A. Aguiar, and A. J. F. N. Sobral, "Gelatin-assisted g-TiO_2/BiOI heterostructure nanocomposites for azo dye degradation under visible light," *Journal of Environmental Chemical Engineering*, vol. 6, no. 4, pp. 4282–4288, 2018.

[12] Y. Tong, C. Zheng, W. Lang et al., "ZnO-embedded BiOI hybrid nanoflakes: synthesis, characterization, and improved photocatalytic properties," *Materials & Design*, vol. 122, pp. 90–101, 2017.

[13] H. Zeynali, S. Behnam Mousavi, and S. M. Hosseinpour-Mashkani, "Synthesis and characterization of Bi/Bi_2S_3 nanocomposite through polyol method and its photovoltaic applications," *Materials Letters*, vol. 144, pp. 65–68, 2015.

[14] C. Yu, J. C. Yu, C. Fan, H. Wen, and S. Hu, "Synthesis and characterization of Pt/BiOI nanoplate catalyst with enhanced activity under visible light irradiation," *Materials Science and Engineering: B*, vol. 166, no. 3, pp. 213–219, 2010.

[15] H. Cheng, B. Huang, Y. Dai, X. Qin, and X. Zhang, "One-step synthesis of the nanostructured AgI/BiOI composites with highly enhanced visible-light photocatalytic performances," *Langmuir*, vol. 26, no. 9, pp. 6618–6624, 2010.

[16] W. J. Kim, D. Pradhan, B.-K. Min, and Y. Sohn, "Adsorption/photocatalytic activity and fundamental natures of BiOCl and $BiOCl_xI_{1-x}$ prepared in water and ethylene glycol environments, and Ag and Au-doping effects," *Applied Catalysis B: Environmental*, vol. 147, pp. 711–725, 2014.

[17] N. T. Hahn, S. Hoang, J. L. Self, and C. B. Mullins, "Spray pyrolysis deposition and photoelectrochemical properties of n-type BiOI nanoplatelet thin films," *ACS Nano*, vol. 6, no. 9, pp. 7712–7722, 2012.

[18] G. Odling and N. Robertson, "SILAR BiOI-sensitized TiO_2 films for visible-light photocatalytic degradation of Rhodamine B and 4 chlorophenol," *ChemPhysChem*, vol. 18, no. 7, pp. 728–735, 2017.

[19] P.-Y. Kuang, J.-R. Ran, Z.-Q. Liu et al., "Enhanced photoelectrocatalytic activity of BiOI nanoplate-zinc oxide nanorod p-n heterojunction," *Chemistry—A European Journal*, vol. 21, no. 43, pp. 15360–15368, 2015.

[20] H. M. Pathan and C. D. Lokhande, "Deposition of metal chalcogenide thin films by successive ionic layer adsorption and reaction (SILAR) method," *Bulletin of Materials Science*, vol. 27, no. 2, pp. 85–111, 2004.

[21] Y. Huang, H. Li, W. Fan et al., "Defect engineering of bismuth oxyiodide by IO_3–doping for increasing charge transport in photocatalysis," *ACS Applied Materials & Interfaces*, vol. 8, no. 41, pp. 27859–27867, 2016.

[22] X. Xiao and W.-D. Zhang, "Facile synthesis of nanostructured BiOI microspheres with high visible light-induced photocatalytic activity," *Journal of Materials Chemistry*, vol. 20, no. 28, pp. 5866–5870, 2010.

[23] D. S. Bhachu, S. J. A. Moniz, S. Sathasivam et al., "Bismuth oxyhalides: synthesis, structure and photoelectrochemical activity," *Chemical Science*, vol. 7, no. 8, pp. 4832–4841, 2016.

[24] M. Zhang, J. Qin, P. Yu et al., "Facile synthesis of a ZnO-BiOI p-n nano-heterojunction with excellent visible-light photocatalytic activity," *Beilstein Journal of Nanotechnology*, vol. 9, pp. 789–800, 2018.

[25] M. Azadi and A. Habibi-Yangjeh, "Microwave-assisted facile one-pot method for preparation of BiOI–ZnO nanocomposites as novel dye adsorbents by synergistic collaboration," *Journal of the Iranian Chemical Society*, vol. 12, no. 5, pp. 909–919, 2015.

[26] L. G. Sillen and S. K. Tidskrift, "Calculated from ICSD using POWD-12++," in *Structure*, vol. 53, ICDS card number 01-073-2062, Integrated Child Development Services, 1997.

[27] R. Y. Korotkov, P. Ricou, and A. J. E. Farran, "Preferred orientations in polycrystalline SnO_2 films grown by atmospheric pressure chemical vapor deposition," *Thin Solid Films*, vol. 502, no. 1-2, pp. 79–87, 2006.

[28] J. Cao, B. Xu, H. Lin, B. Luo, and S. Chen, "Novel heterostructured Bi_2S_3/BiOI photocatalyst: facile preparation, characterization and visible light photocatalytic performance," *Dalton Transactions*, vol. 41, no. 37, pp. 11482–11490, 2012.

[29] B. D. Cullity, *Elements of X-ray Diffraction*, Addison-Wesley Company, Boston, MA, USA, 1978.
[30] K. M. Reddy, S. V. Manorama, and A. R. Reddy, "Bandgap studies on anatase titanium dioxide nanoparticles," *Materials Chemistry and Physics*, vol. 78, no. 1, pp. 239–245, 2003.
[31] W.-W. Dai and Z. Yan Zhao, "Electronic structure and optical properties of BiOI as a photocatalyst driven by visible light," *Catalysts*, vol. 6, no. 9, p. 133, 2016.